FRAGMENTATION AND SPREADING OF A METEOR-LIKE OBJECT

Chul Park[1] and Jeffrey D. Brown[2]

[1] Department of Aerospace Engineering Korea Advanced Institute of Science and Technology, Daejeon 305-701, Republic of Korea
[2] ERC, Inc., Moffett Field, CA 94035, USA

ABSTRACT

The phenomenon of fragmentation and spreading of a high-speed flying object resembling a meteorite is studied experimentally and theoretically. Experimentally, a model made of graphite is launched in a ballistic range and is made to fragment and spread. The flow field produced by the cloud of the fragments is observed optically. The observed deceleration and spreading behavior is numerically reconstructed using computational-fluid-dynamic calculations, applying an improved meteoroid fragmentation theory. The existing meteoroid fragmentation theory is improved by introducing the hypothesis that the incubation process of the pressurized fluid permeating through the fragment precedes the splitting process. The incubation time is determined by the ratio of permeability of the fragment to the fluid's viscosity and is much longer than the time for splitting given by the existing theory. Agreement is obtained between the observed and calculated behavior of the fragment cloud by appropriately choosing this ratio.

Key word: meteorites, meteors, meteoroids

Online-only material: color figures

1. INTRODUCTION

How a meteor breaks up, fragments into small pieces, ablates, and decelerates has been a subject of serious study in recent years. Traditionally, this subject has been studied to predict the damage caused by the impact of a meteor on the ground. Recently, it gained attention in relation to the question as to whether the building blocks of life could have been seeded from outer space.

It is now believed that a meteoroid breaks up first because of the stresses built up due to the different aerodynamic forces exerted on different parts of the meteoroid. After the initial breakup, the aerodynamic interactions between the neighboring fragments produce aerodynamic forces that push these fragments apart: two supersonic objects located laterally closely produce a repulsive lateral force between them because of the interaction of shock waves (Artem'eva & Shuvalov 1996; Zhdan et al. 2004). Fragmentation continues and the fragments become smaller as the entry flight progresses, and, consequently, decelerates faster. At the same time, the fragments spread. How these phenomena occur will decide how much damage will be done to the ground or how likely it is for the extraterrestrial building blocks of life to survive entry flights.

For this reason, it is desirable that the fragmentation and spreading phenomena of a hypersonic body be observed in a ground-based laboratory. By serendipity, such experimental data were obtained in a ballistic range. In the present work, these experimental data are presented. The existing theory on the fragmentation of meteoroids is extended and applied to numerically recreate the observed data. A computational-fluid-dynamics (CFD) calculation was made of the flow field produced by the spatially distributed cloud of fragments.

The rate of fragmentation is seen to be much slower than predicted by the prevailing theory (Passey & Melosh 1980; Hills & Goda 1993). In order to reconcile this discrepancy, a hypothesis was made that the pressurized fluid in the stagnation region must permeate through a fresh fragment in order to cause it to split. This time, called incubation time in the present work, is controlled by the ratio of permeability of the fragment to the fluid's viscosity and calculated to be much longer than the time for it to split mechanically. By choosing this ratio value appropriately, the present work shows that agreement can be achieved between the theory and the experimental data obtained in the ballistic range.

2. BALLISTIC RANGE EXPERIMENT

The aforementioned experiment was conducted at the Hypersonic Free-Flight Range Facility of NASA Ames Research Center (Park & De Rose 1980). A model made of industrial-grade graphite was launched in this facility to a speed of about 4 km s^{-1}. This graphite was made by binding graphite particles with an organic resin. The model was made to fly through a chamber filled with krypton or xenon to a pressure of 200 torr. The purpose of the experiment was to observe the radiation emitted by the hot krypton or xenon surrounding the model. Figure 1 shows the general experimental setup.

The rest of the range was filled with air to 100 torr. The krypton/xenon chamber, located in Region 2 in Figure 1, had an overall length of 270 cm. A total of 11 shots, Shots 1536 through 1546, were made. Of these, five, Shots 1539 through 1543, were performed with a model made of graphite, which showed the breaking up and spreading phenomena. The models, 1.905 cm in diameter, were in the shape of the *Galileo* probe vehicle, which entered Jupiter in 1995 (Park 2009) and weighed 8 g. The two ends of the krypton/xenon chamber were covered with a diaphragm made of 0.0127 mm thick Mylar. The models were launched with a two-stage light-gas gun. The models broke through the two diaphragms, and, emerging out of the chamber, flew through the rest of the range designated as Region 3 in Figure 1. Shadowgraph pictures were taken through the 27.5 cm diameter windows located at intervals of 1.524 m. Flight speed was determined from the locations of the model determined from the shadowgraphs and the timing record of the shadowgraphs. For the five shots mentioned, the initial velocity of the model while inside the Region 2 chamber varied from 3.850 to 4.520 km s^{-1}. Park & De Rose (1980) reported the phenomenon observed in the krypton/xenon chamber. The flux

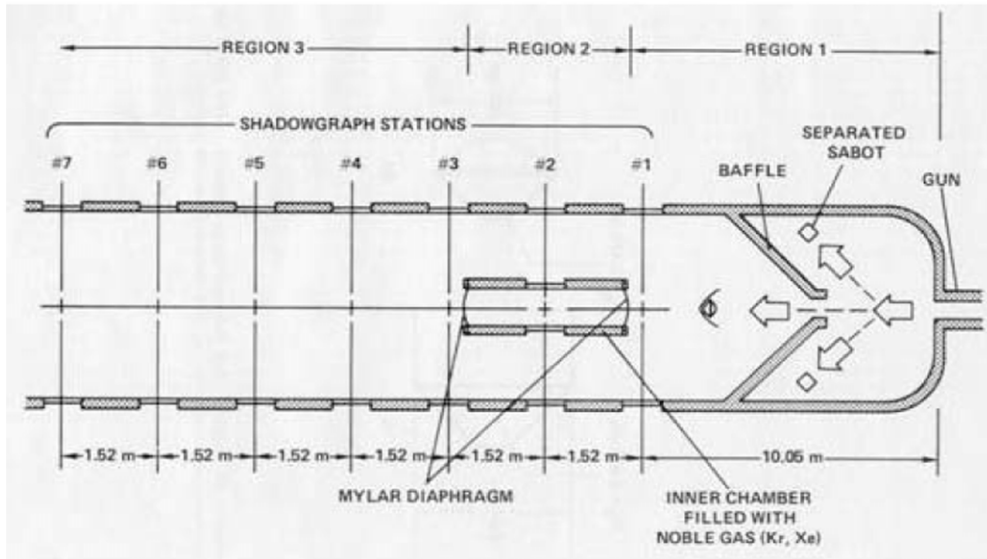**Figure 1.** Schematic of ballistic range setup.

Table 1
Measured and Calculated Parameters of Ballistic Range Shot 1543

Known values	
Local air density	0.1577 kg m^{-3}
Fragment material density assumed	2000 kg m^{-3}
Fragment total mass	8×10^{-3} kg
Initial fragment radius r_0 assumed	3.5×10^{-5} m
Total number of fragments corresponding to assumed r_0	2.227×10^7
Number density of fragments corresponding to assumed r_0	1.485×10^{11} m^{-3}
At $t = 0$ s	
Distance from reference point	0 m
Measured velocity	4200 m s^{-1}
Fragment cloud radius measured	0.033 m $\pm$ 10%
At $t = 6.60 \times 10^{-4}$ s	
Distance from xenon chamber exit	1.600 m
Calculated velocity	1636 m s^{-1}
Fragment cloud radius measured	0.055 m $\pm$ 10%
At $t = 2.78 \times 10^{-3}$ s	
Distance from reference point	3.110 m
Calculated velocity	346 m s^{-1}
Fragment cloud radius measured	0.130 m $\pm$ 10%

of radiative power incident in the model and the stagnation pressure were calculated to be of the order of 200 kW cm^{-2} and 250 (with xenon) atm.

The parameters of the serendipitous Shot 1543, some measured and some calculated, are presented in Table 1. In Figures 2(a) through (d), the shadowgraphs taken in Shot 1543 are shown. In the picture shown in Figure 2(a), the number 1S-1543 signifies that the picture was taken through the side window in Station 1 in Shot 1543. In Figure 2(a), the model is intact. In Figure 2(b), a luminosity picture is taken of the model flying through xenon. The four-level graded image at the top is a luminosity calibration exposure. There is no picture at Station 3. For this shot, the shutter on the camera failed to open, but the arrival time of the model was successfully captured.

In Figure 2(c), the shadowgraph taken at Station 4 is shown. Here, the model is broken into small pieces and fragments are spread over a diameter of the order of 12 cm, six times the model's diameter. In Figure 2(d), a cloud is seen at Station 5. The

white appearance signifies that the light is blocked. The blocking of light is only by solid particles: there is no known optical absorption by air or possible compound between air and carbon, i.e., CO and NO, in the visible wavelength range. Therefore, one can conclude that the fragmentation produced many very small solid particles: the model was totally pulverized. The diameter of the fragment cloud is approximately equal to the diameter of the window, i.e., about 28 cm.

For the four remaining graphite shots, shadowgraphs were successfully taken at Station 3. One of them, Shot 1540, is shown in Figure 3. As seen here, the model seems to be exploding. All four shadowgraphs showed exactly the same feature. The diameters of the envelopes of the exploding bodies were nearly the same, 6.6 ± 1.5 cm, roughly 3.5 times the diameter of the model. It is assumed that the same occurred for Shot 1543.

Why this "explosion" occurred at the exit of the krypton/xenon chamber is unknown. One could speculate that the phenomenon is due to the combination or interaction between (1) the mechanical shock exerted on the model in breaking the Mylar diaphragm on exiting from the chamber, (2) the sudden drop of the stagnation pressure from 250 atm inside the chamber to about 25 atm outside the chamber, and (3) rapid vaporization of the resin within graphite heated inside the xenon chamber. Somehow, the intense heat and the high pressure produced by the shock layer in the xenon chamber, and the process of passing through the diaphragm, caused this initial breakup. The initial breakup seemingly caused the fragments to fly apart almost radially. The transverse velocity of the observed cloud at the outer edge of the cloud is named V_0 here. This V_0 is unique to the experiment and cannot be calculated with any existing theory.

Thus, for Shot 1543, for some reason the model was fragmented extensively: no single piece contained any meaningful fraction of the total mass. The fragments formed a cloud-like appearance, and the diameter of this cloud expanded. For the other four shots, the breakup occurred but not so extensively. Figure 4 shows an example. As shown in Figure 4, even though the fragmentation is not extensive, the fragments spread laterally. The distances between the neighboring fragments are substantially larger than the diameter of each fragment.

(a)

(b)

(c)

(d)
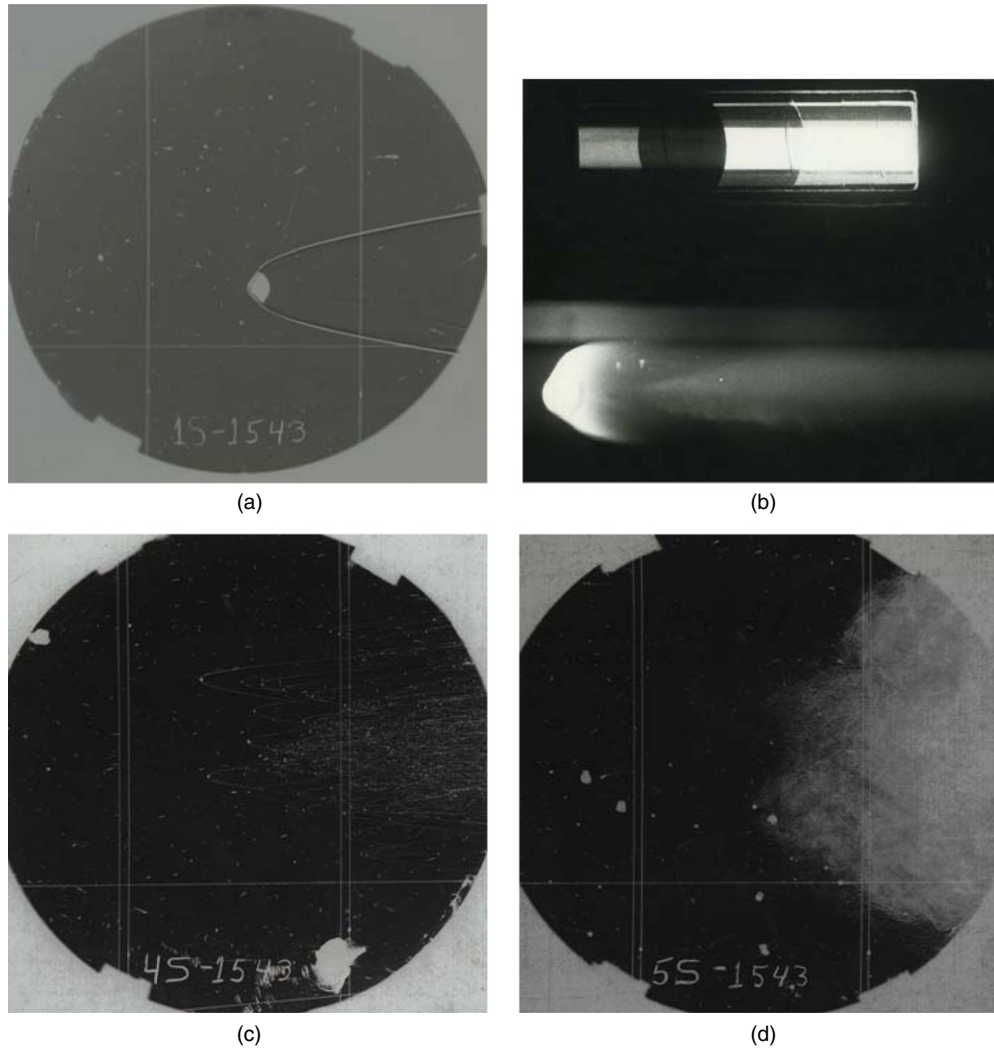
Figure 2. Shot 1543. (a) Shadowgraph at Station 1. (b) Luminosity photograph at Station 2. (c) Shadowgraph at Station 4. (d) Shadowgraph at Station 5.
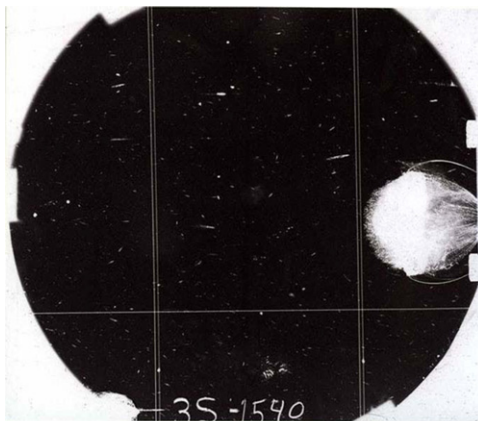

Figure 3. Shot 1540, Station 3.
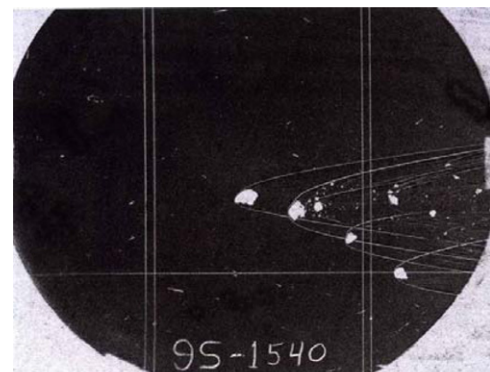
Figure 4. Shot 1540, Station 9.

3. FRAGMENTATION MODELING

In order to simplify the analysis, it is assumed in the present work that (1) the model was fragmented to form spheres of the same radius, (2) these spheres are uniformly distributed spatially, and (3) these spherical fragments move with a transverse velocity component V that is proportional to the radial distance from the axis of symmetry R of each fragment.

The V-value for the outermost fragments at the beginning is V_0. The density of graphite is taken to be 2000 kg m^{-3}. Because the total mass of the fragments is known to be 8 g, by assuming the initial (at the exit of xenon chamber) radius of the fragments r_0, the number density and total number of fragments at the beginning are fixed.

The process of subsequent repeated fragmentation could be described conceptually by what is termed the "Medusa's head" model by Levin & Bronshten (1986), shown in a slightly
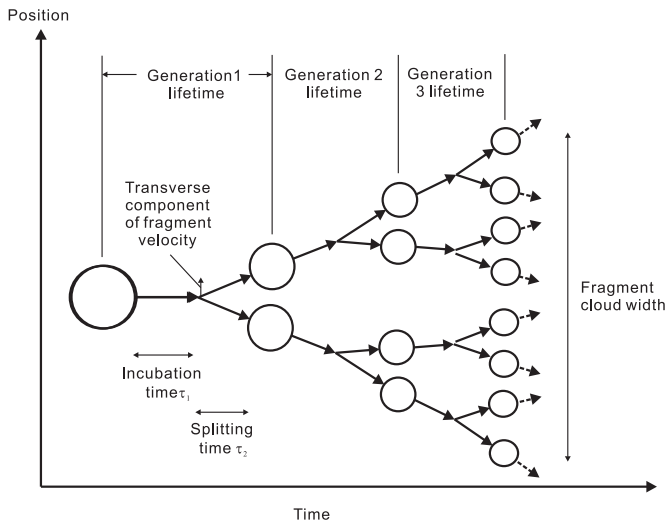
Figure 5. Conceptual description of progressive fragmentation process termed "Medusa's head" model (Levin & Bronshten 1986).

modified form in Figure 5. As shown in Figure 5, conceptually, fragmentation occurs in discrete stages or generations, all fragments in unison. In this staged generation description, a generation begets a next generation through one discrete burst.

In reality, fragmentation does not occur in unison: different fragments have different diameters and so the times for begetting the next generation differ. For this reason, fragmentation is assumed to be continuous in the present work, and its rate is expressed by

$$\frac{d}{dt}(\ln n) = 1/\tau, \qquad (1)$$

where τ is the characteristic fragmentation time constant. This means that the number density n increases as $\exp(t/\tau)$. Baldwin & Sheaffer (1971) hypothesized that a meteoroid breaks up in one burst into about eight fragments. The photograph taken of the Moravka meteorite (Borovicka & Kalenda 2003) shows seven major fragments, in close agreement with this hypothesis. In order to reconcile the continuous fragmentation model, Equation (1), with this hypothesis, one fragmentation event must be considered to occur in the time span of $\ln(8) = 2.079$ times τ. To maintain simplicity, this is truncated to 2, so that one burst of fragmentation is taken to occur over a time span of 2τ: one fragment splits into $e^2 = 7.389$ fragments in a time of 2τ.

Passey & Melosh (1980) and Hills & Goda (1993) developed the discrete fragmentation model in finer detail. The original "Medusa's head" model assumes that the life span of one generation consists of the time for splitting, shown as τ_2 in Figure 5. This τ_2 is usually very short, and so this hypothesis led Hills & Goda (1993) to predict that most meteorites will fragment, decelerate, and ablate away very rapidly. As will be shown later, the present ballistic range data does not support this hypothesis: the observed fragmentation rate is much slower.

In order to reconcile this discrepancy, the time for incubation of the splitting event, τ_1, is hypothesized and added in the present work, as indicated in Figure 5. Thus, according to the present model,

$$\text{Generation lifetime} = 2\tau = \tau_1 + \tau_2. \qquad (2)$$

The nature of the incubation phenomenon will differ according to the type of the meteoroid and the flight regime. For a substantially large (larger than, say 1 m) asteroidal meteoroid, initially the meteoroid will be broken up by the stress caused
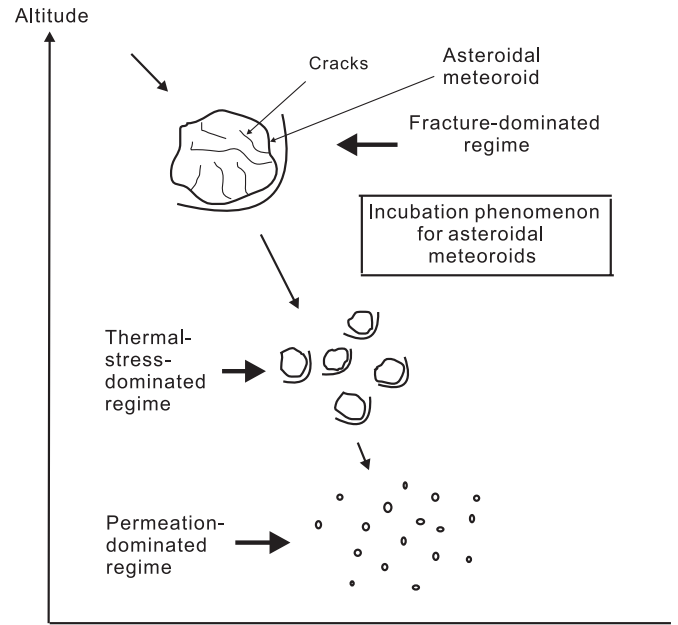
(a)
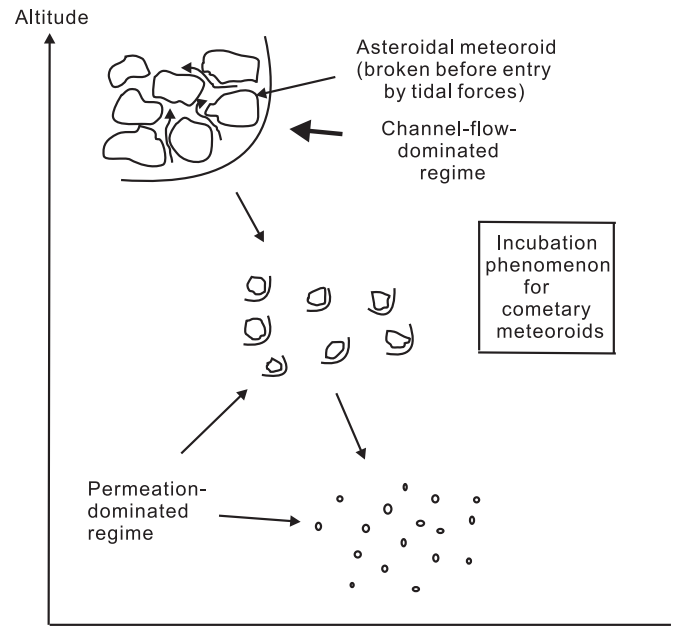
(b)

Figure 6. Conceptual classification of incubation phenomenon. (a) Asteroidal meteoroid. (b) Cometary meteoroid.

by pressure. Cracks will be generated and air and the product of vaporization of the meteoroid will travel through these cracks, as shown schematically in Figure 6(a). The meteoroid, consisting mostly of stones and iron, will also melt and produce liquid substances on its surface, which will flow relatively slowly along the surface. The phenomenon can be identified as the incubation process for this flight regime. After the fragments are broken into smaller pieces (say, to sizes of 10 cm), each fragment will likely be free of cracks. The thermal shock phenomenon will dominate in this regime. Damage mechanics, such as that described by Ashby & Sammis (1990), is applicable to these two regimes. Still later, when the fragments attain subcentimeter sizes, a phenomenon named here the "permeation
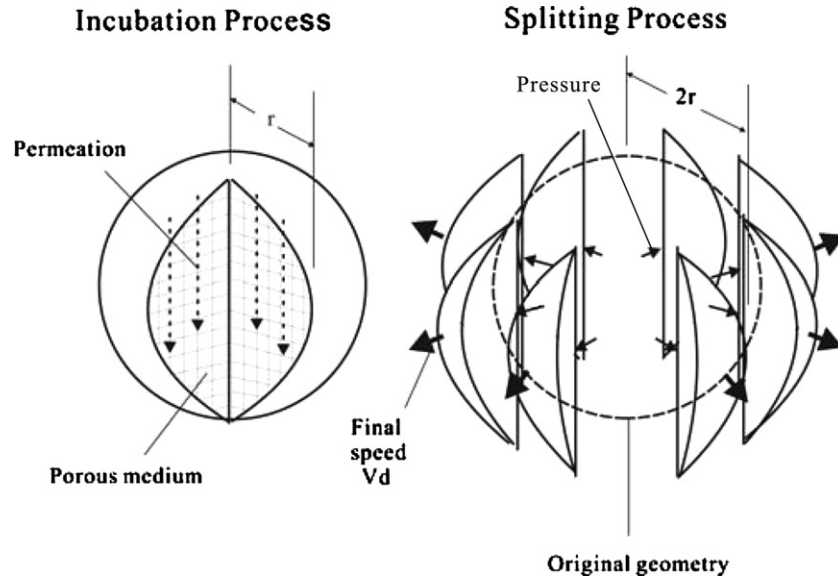
Incubation Process

Splitting Process

Figure 7. Schematic of the two processes in fragmentation.

phenomenon" will dominate, which will be described in detail later.

For a cometary meteoroid, a different phenomenon will occur. When a cometary meteoroid of substantial size enters Earth's atmosphere, it is most likely already broken into many lumps, as illustrated in Figure 6(b), because of the tidal forces of the Sun and Earth. High pressure will pass through the openings between the neighboring lumps, called channels in Figure 6(b). The heat will melt the meteoroid, and the melted part will flow inside the channels. When the fragment's size becomes of the order of 1 m or less, the permeation phenomenon mentioned above will dominate. By this time, the fragments have been thoroughly soaked in the melted part of the meteoroid and lack the rigidity to produce mechanical fracture. Instead, a new high-pressure melt passes through the body. This process constitutes the incubation phenomenon in this regime.

The phenomenon of the high-pressure melt passing through the fragment, depicted schematically in the left side of Figure 7 marked "Incubation process," is of interest in the present work because the tiny fragments observed in the ballistic range experiment described above are in this regime.

According to Passey & Melosh (1980) and Hills & Goda (1993), the splitting time τ_2 can be deduced approximately from the energy considerations. The force that pushes two fragments apart sideways is the aerodynamic force that is approximately the stagnation pressure times the cross-sectional area of the fragment. The aerodynamic force exists until the two bodies are separated by about the radius of the original fragments, as shown schematically in the right side figure of Figure 7. The work done in this way can be expressed as

$$\text{Work} = \text{Force} \times \text{distance}$$
$$\approx \rho U^2 \int_r^{2r} \pi r^2 dr = \frac{7}{3}\pi\rho U^2 r,$$

where ρ is the density of air, U is the flight velocity, and r is the radius of the fragment before splitting. Equating this work to the kinetic energy of the fragments, one has (Hills & Goda 1993)

$$\frac{1}{2}\left(\frac{4}{3}\pi\rho_s r^3\right) V_d \approx \frac{7}{3}\pi\rho U^2 r^3, \qquad (3)$$

where ρ_s is the density of the fragment and V_d is the lateral velocity after splitting. Solving Equation (3) for V_d, one obtains

$$V_d = \left(\frac{7\rho}{2\rho_s}\right)^{1/2} U \approx 2\left(\frac{\rho}{\rho_s}\right)^{1/2} U. \qquad (4)$$

Because the force pushing the fragments is $\rho U^2 \pi r^2$ and the mass of the fragment is $(4/3)\pi r^3 \rho_s$, the equation of motion can be written as

$$r\frac{d^2 r}{dt^2} = \frac{3}{4}\frac{\rho}{\rho_s} U^2.$$

One must solve this equation to obtain the time taken τ_2 for r to increase from r to $2r$. However, because this equation is nonlinear, no closed-form solution can be found. In order to derive an approximate closed form solution, the equation is linearized by assuming the factor r in the left-hand side to have an average value of $1.5r$, where r in this case is a fixed value. Then the solution leads to

$$\tau_2 \approx \left(\frac{\rho_s}{\rho}\right)^{1/2} \frac{r}{U}. \qquad (5)$$

In the permeation-dominated regime under consideration, the incubation time τ_1 is the time required for the pressurized fluid in the stagnation region to penetrate into the porous fragment. According to Darcy's law, in a steady state, the flow velocity through a porous medium is describable by

$$u = -\frac{K}{\mu}\frac{dp}{dx},$$

where K is permeability, μ is the viscosity of the fluid permeating through the porous body, and p and x are the pressure and the penetrating distance, respectively. Approximating dp/dx by $-\rho U^2/(2r)$, one has the incubation time τ_1 of

$$\tau_1 \approx \frac{2r}{u} = \frac{\mu}{K}\frac{4r^2}{\rho U^2}. \qquad (6)$$

Thus, τ_1 is inversely proportional to the ratio K/μ. A similar result was found by Shuvalov & Trubetskaya (2010): using

a detailed computer code named SOVA, they found that the so-called internal friction influences the deformation of a damaged meteoroid. The ratio K/μ is left in the present work as an adjustable parameter and varied until the theory agrees with the experiment.

As mentioned, the lateral velocity of the fragments increased in one stage of fragmentation, i.e., over a time span of 2τ, which is given by Equation (4). Over the time span of Δt, the increment in the lateral velocity of a fragment, ΔV_d, becomes

$$\Delta V_d = 2 \left(\frac{\rho}{\rho_s}\right)^{1/2} U \frac{\Delta t}{2\tau}.$$

In reality, this value must be divided by two, because V_d is the velocity relative to other fragments instead of the original body depicted in the right side figure in Figure 7,

$$\Delta V_d = \frac{1}{2} \left(\frac{\rho}{\rho_s}\right)^{1/2} U \frac{\Delta t}{\tau}. \tag{7}$$

Equation (7) applies to the fragment located at the outer edge of the fragment cloud. For the fragments inside the cloud, one can assume a proportional distribution. By denoting the lateral distance by R and its edge value by R_e, one can write

$$\Delta V = \Delta V_d \times \frac{R}{R_e} = \frac{1}{2} \left(\frac{\rho}{\rho_s}\right)^{1/2} U \frac{\Delta t}{\tau} \frac{R}{R_e}. \tag{8}$$

4. FLOW-FIELD MODELING

As mentioned, we consider an aggregate of small fragments in which the fragments are separated by distances larger than the diameters of the fragments. The aggregate of the fragments will henceforth be called the fragment cloud. The fragments inside the fragment cloud are flying through the air at a high speed. Each fragment will generate a bow shock wave, which will extend to some distances downstream, as can be seen in Figure 2(a). Drag is produced by this phenomenon. At a large distance downstream of the fragment, the lingering effect of one fragment will be a decrease in the momentum of the air flow in the direction of motion. The momentum decrement per unit volume will equal the sum of the drag forces produced by all fragments contained in the volume.

Assuming that the distances between neighboring fragments are large, there will be no sidewise forces between neighboring fragments. However, sidewise force will be generated indirectly though weakly. The flow momentum change in the flow direction will produce a non-uniform flow over the fragment cloud: pressure will be high in the middle of the cloud and low in the periphery of the cloud. The resulting pressure gradients will generate sidewise forces to the fragments.

The radii of the fragments r and number density of the fragments n are taken to be functions of location. They are assumed initially to be the same everywhere inside the cloud. The cloud is assumed to have a spherical shape in the beginning; it changes shape during the flight, but is assumed to remain axially symmetric throughout.

For a meteoroid in the atmosphere, the flow formed by the fragment cloud will be very hot. Dissociation and ionization phenomena must be considered for that flow. However, for the ballistic range experiment in the present work, the flow properties, i.e., pressure and density, can be approximated by the perfect gas assumption for the following reasons: Even though

the starting velocity was about $4\,\mathrm{km\,s^{-1}}$, the model decelerated rapidly and flew most of the observed range at a low hypersonic or supersonic speed. The fragments were too small to produce an equilibrium region behind their individual bow shock waves, and so the molecules hitting the fragment's surfaces were N_2 and O_2. Therefore, no oxidation or nitridation was possible. Radiative heating was negligible. The convective heating rates were such that the radiation equilibrium temperature, i.e., the temperature at which the convective heat transfer rate and the blackbody radiation flux are equal, remained below the sublimation temperature. As a result, sublimation was also negligible. Thus, no ablation occurred for the fragments in the ballistic range experiment.

To determine the forces acting on each fragment, CFD calculation is carried out. From the velocity vectors calculated in this manner, magnitude and direction of the drag force of the fragment located at the grid point are calculated. The drag of one fragment at the grid point times the local number density n gives the drag force applied to the flow per unit volume around that grid point. Drag force is calculated from the radius of fragment r assuming a drag coefficient of unity. Thus,

$$\text{Drag per unit volume} = \frac{1}{2}\rho W^2 \pi r^2 n,$$

where W is the magnitude of the air-relative velocity.

The motion of the fragment is calculated by integrating the equation of motion of the fragment. At a chosen Δt later, the fragment cloud is at a different location and has a different velocity. The CFD calculation is repeated at this new condition, and so on. A simple trapezoidal integration is performed in the integration of the equation of motion for each fragment.

The flow field over the cloud of fragments is calculated numerically by solving a modified Euler equation for an axisymmetric flow. For the momentum equation, the right-hand sides contained the drag force caused by the fragment cloud. The tangential and transverse components of this drag force constitute the right-hand sides of the two momentum equations.

The boundary conditions are: (1) the inflow is the freestream; (2) along the axis of symmetry, the symmetry assumption is applied; (3) along the outer edge, the freestream conditions are imposed; and (4) along the exit line, the well-known supersonic outflow condition is applied.

Two different computer codes were used in the present work. The first is a generic hypersonic flow solver using an AUSM-DV scheme and the lower–upper Gauss–Seidel sweep method widely used within the aerospace community (e.g., Yamamoto 2004), which is named here, for the purpose of identification, METEOR. This code assumes that the flow is steady, and a time-asymptotic solution is sought. The viscous part of the code was turned off and the code was run as an inviscid flow solver. No artificial damping mechanism is added. The size of the grid was 61×151. The Courant–Friedrich–Levy (CFL) number was set at 0.001. Thirty-one time steps were made along the flight path. The computation was made on a personal computer equipped with four central processing units. 50,000 iterations were made at each time point. A total of 7.5 hr was expended to obtain a solution for the 31 time points. The runs were successful, and the results were used in the present work.

The second code used is the ZEUS code, which is widely used within the astrophysics community (e.g., Stone & Norman 1992). This code is for an inviscid flow and is time accurate. Artificial viscosity is added to stabilize the solution. A minor modification was made to the code to solve the present problem.
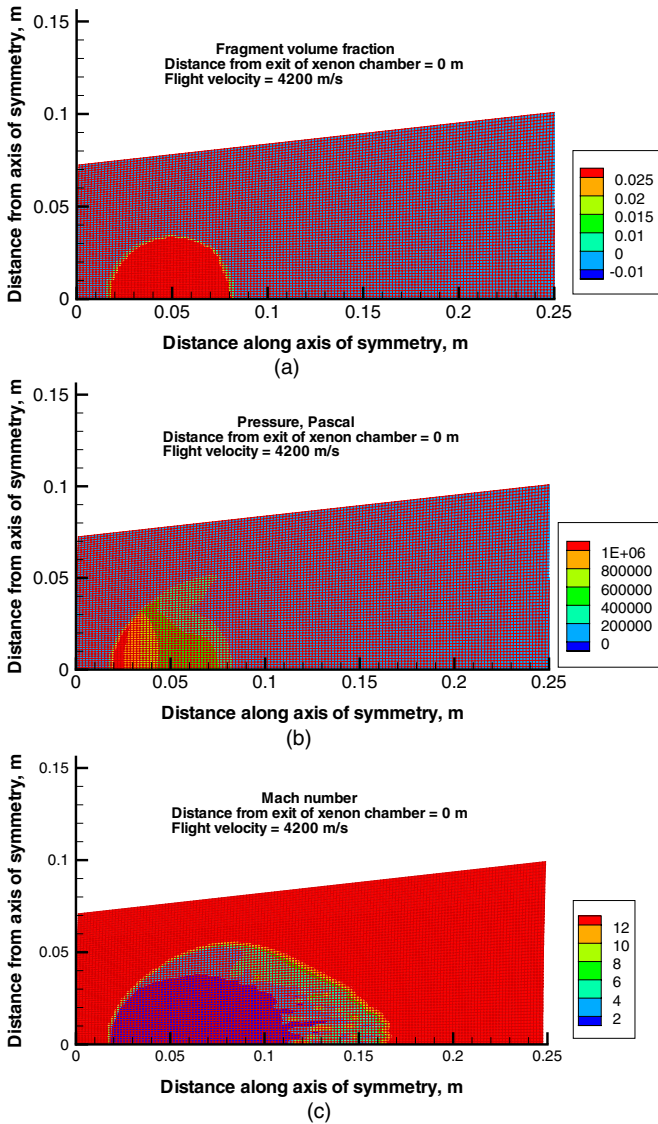
Figure 8. Flow behavior at the exit of xenon chamber; $r_0 = 3.5 \times 10^{-5}$ m, $V_0 = 20$ m s^{-1}, and $K/\mu = 3.0 \times 10^{-12}$ m^4 (N s)$^{-1}$. (a) Fragment volume fraction. (b) Pressure. (c) Mach number.

(A color version of this figure is available in the online journal.)

The modification consisted of adding a "dusty flow" option to the several options already available in the code. The meteor fragments are considered to be very small dust particles, and the drag produced by these particles is accounted for in the way described above. A grid with 256 mesh points in the axial direction and 128 mesh points in the radial direction was used. The CFL number was varied from the recommended value of 0.5 to an extreme value of 0.001. The computation was also made on a personal computer. A clock time of about 30 minutes was expended for a single case. As will be described later, the runs were not successful.

5. RESULTS FROM METEOR CODE

The problem at hand has three unknown parameters: (1) the initial radius of fragments r_0, (2) the initial spreading velocity V_0, and (3) the ratio K/μ. These three parameters are changed in a trial-and-error fashion to arrive at the values that most closely reproduce the experimental data. This selection process is aided by the knowledge that (1) r_0 mainly controls how fast
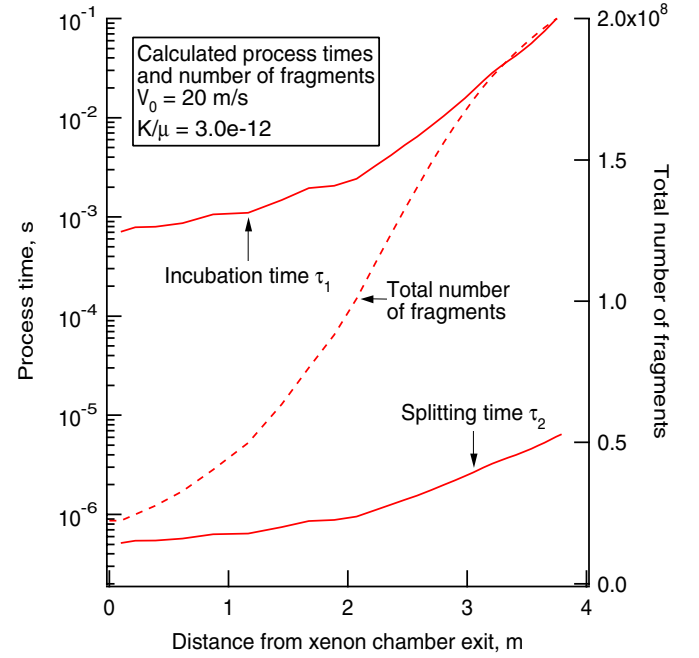
Figure 9. Calculated process times and number of fragments vs. flight distance; $r_0 = 3.5 \times 10^{-5}$ m, $V_0 = 20$ m s^{-1}, and $K/\mu = 3.0 \times 10^{-12}$ m^4 (N s)$^{-1}$.

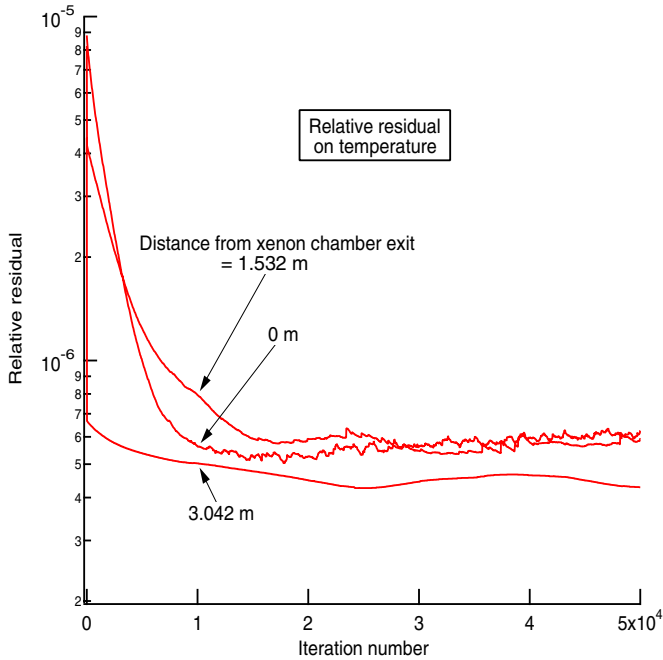(A color version of this figure is available in the online journal.)

the fragments decelerate, (2) V_0 mainly controls the width of the fragment cloud at the distance of 1.5 m downstream of the xenon chamber exit (see Figure 2(c)), and (3) K/μ mainly controls the width of the fragment cloud at the distance of 3 m downstream of the xenon chamber exit (see Figure 2(d)).

The results of the METEOR code are as follows. The best values chosen are: 3.5×10^{-5} m for r_0, 20 m s^{-1} for V_0, and 3×10^{-12} m^4 (N s)$^{-1}$ for K/μ. Table 1 summarizes the characteristic values derived from these three parameters. In the following, the process of determining these values is explained.

An example of the calculated flow fields is shown in Figures 8(a)–(c). These figures show the distribution of fragment volume fractions, pressure distribution, and Mach number distribution at the xenon chamber exit. These figures show that a flow field resembling that over a solid body develops. The solution is seemingly rough in the afterbody region. This is probably due to the oscillation. The afterbody flow is possibly unsteady. The present procedure of seeking a time-asymptotic steady-state solution may suffer from this intrinsic unsteadiness of the afterbody flow. Fortunately, this unsteadiness does not affect the location and width of the fragment cloud being sought here.

Figure 9 shows the variation of the calculated total number of fragments and the two process times, τ_1 and τ_2, along the flight path for the chosen parameter set. The total number increases by an order of magnitude within the observed 3 m. The incubation time τ_1 is orders of magnitude larger than the splitting time τ_2. This is the main difference between the model of Hills & Goda (1993) and the present work. The Hills & Goda model hypothesized that the fragmentation time equals the splitting time τ_2. That model would dictate that the total number of fragments will increase much more rapidly than calculated in the present work, and will disagree with the experimental observation.

Figure 10 shows the convergence behavior of the CFD solutions. As shown in the figure, the convergence is not very

Figure 10. Relative residual vs. iteration number; $r_0 = 3.5 \times 10^{-5}$ m, $V_0 = 20$ m s^{-1}, and $K/\mu = 3.0 \times 10^{-12}$ m^4 (N s)$^{-1}$.

(A color version of this figure is available in the online journal.)

Figure 11. Position of the fragment cloud for different r_0; $V_0 = 20$ m s^{-1} and $K/\mu = 3.0 \times 10^{-12}$ m^4 (N s)$^{-1}$.

(A color version of this figure is available in the online journal.)

good. This is probably again due to the fact that the flow oscillates in the downstream region.

In Figure 11, the calculated positions of the fragment cloud are compared with the experimental data for two different values of r_0, 3.5×10^{-5} and 7.0×10^{-5} m, while V_0 and K/μ are kept fixed. The calculations for r_0 smaller than 3.5×10^{-5} m are not shown because those cases led to a divergence of number densities and consequently no meaningful CFD solutions. As can be seen, the experimental data are fitted with r_0 of 3.5×10^{-5} m. Several solutions are also obtained with different values of V_0 and K/μ while maintaining $r_0 = 3.5 \times 10^{-5}$ m. All such solutions gave results close to the one shown.

In Figures 12(a)–(c), the calculated values of the radius of the fragment cloud are compared with the experimental data while r_0 is fixed as 3.5×10^{-5} m. In Figure 12(a), K/μ is varied while V_0 is fixed. As can be seen, the K/μ value of 3.0×10^{-12} m^4 (N s)$^{-1}$ fits the experimental data best. In Figure 12(b), V_0 is varied. As can be seen, $V_0 = 20$ m s^{-1} best fits the experimental data. In Figure 12(c), an effort is made to fit the experimental data by simultaneously varying K/μ and V_0. As is shown, no such combination of values significantly different from the chosen values can be found.

6. RESULTS FROM THE ZEUS CODE

The ZEUS code calculates the temporal changes in the flow field accurately. To do so, the time step is changed automatically in the code. For the present problem, the time step decreases steadily until it reaches unrealistically small values, presumably because of the intrinsically unsteady nature of the flow field. At a certain point, the numerical truncation errors overwhelm and the code stops citing an excessively large number of errors.

What happens at the point of stopping can be seen in Figure 13, which shows the pressure distribution. This figure contrasts to Figure 8(b), which shows the pressure distribution calculated by the METEOR code. The general features of the
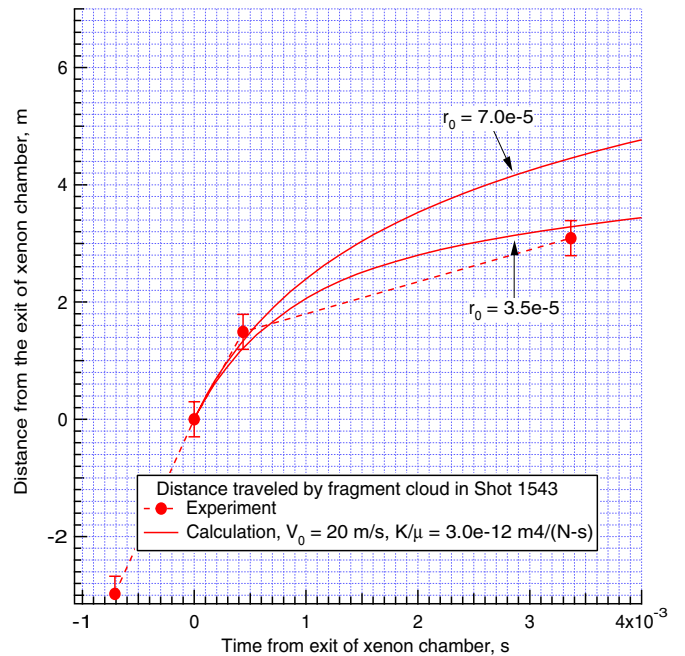
flow field are similar between the two solutions. However, in the ZEUS solution, a complicated flow field develops in the central region of the fragment cloud, and the pressure climbs to a high value therein. Such high pressure cannot be physically real and is believed to be due to some unknown problems in the code such as artificial viscosity. Artificial viscosity was varied in the calculation from the recommended value of 2 to 0.2, 1, and 4. The stopping time points were earlier with these different artificial viscosity values. The CFL number was varied from the recommended value of 0.5 to as low as 0.01. No difference was seen. An effort must be undertaken in the future by persons more familiar with this code to remove this obstacle before the code can be used for this problem.

7. DISCUSSION

In the present work, the two characteristic times for fragmentation, τ_1 and τ_2, are derived using simple assumptions. To be more precise, one could introduce adjustable multiplicative factors for these two times if one had more experimental data to calibrate those factors with. In the absence of such experimental data, such finer adjustment would seem unwarranted. One hopes that more experiments of the kind described in the present work will be made in the future to enable calibration of a more precise theoretical model.

For the graphite model tested in the present work, the most likely value of K/μ is found to be 3×10^{-12} N s m^{-4}. What this value implies is now examined. When heated, the industrial-grade graphite used in the ballistic range experiment loses its volatile resin component by evaporation and becomes porous. At room temperature, water has a viscosity of about 2×10^{-3} N s m^{-2}. The melted liquid of the resin binding the graphite model may have a somewhat higher viscosity, perhaps 10^{-2} N s m^{-2}. The K/μ value of 3×10^{-12} implies a K-value of about 3×10^{-14} N s m^{-2}. This value of K is that of a typical rock. The graphite used in the experiment when heated and
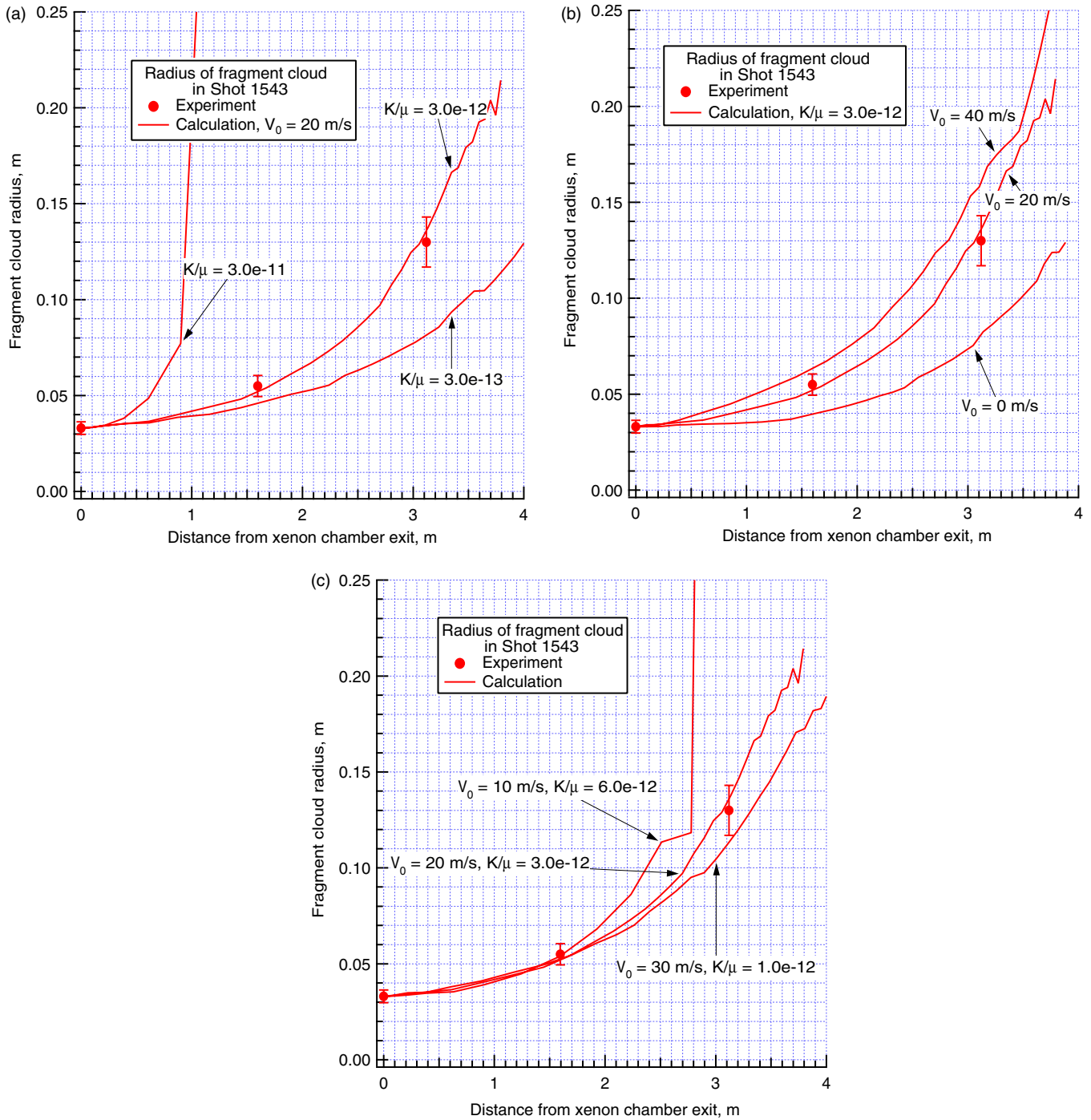
Figure 12. Radius of the fragment cloud for $r_0 = 3.5 \times 10^{-5}$ m. (a) For different K/μ with $V_0 = 20$ m s^{-1}. (b) For different V_0 with $K/\mu = 3.0 \times 10^{-12}$ m^4 (N s)$^{-1}$. (c) With simultaneously changed V_0 and K/μ.

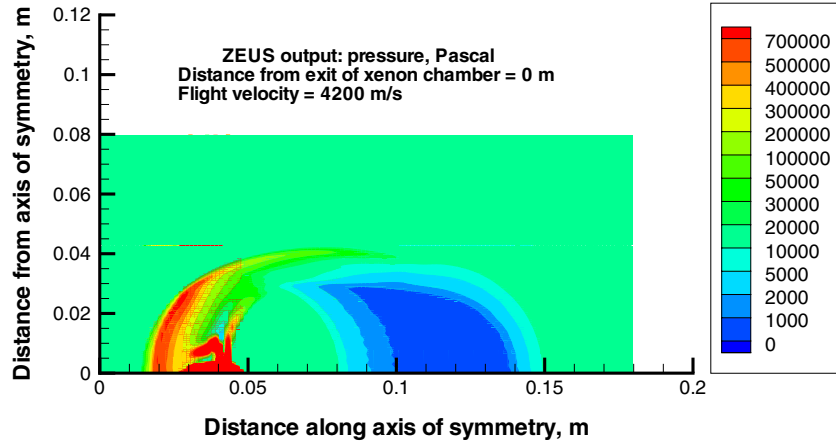(A color version of this figure is available in the online journal.)

thereby made porous may have such a value of K, and therefore the K/μ value deduced in the present work seems plausible.

A question arises as to whether the fragment is internally empty prior to permeation of the pressurized fluid, i.e., whether the void inside the fragment is filled with a liquid. A freshly cut fragment should be considered empty because the pressure built up during the preceding generation is likely to be discharged during the process of splitting.

The present results show that the fragmentation rate is dictated mostly by what is called an incubation time. The incubation time is hypothesized in the present work to be the time for

the pressurized fluid to permeate through the fragment and thus cause its inflation and fracture. As shown in Figure 9, if this incubation time is not accounted for, then fragmentation is predicted to occur with an orders-of-magnitude-faster rate than observed. Because τ_1 scales as r^2 while τ_2 scales as r, the incubation time will tend to become more dominant for larger meteoroids. As mentioned, this theory applies only to relatively small bodies.

Although the motivation for the present work was to predict the behavior of cometary meteoroids, the experimental sample, graphite, more resembles a stony asteroidal meteoroid.

Figure 13. Pressure distribution at $t = 0$ s; ZEUS solution when the code stops because of too many errors; computing time $= 1.54 \times 10^{-3}$ s.

(A color version of this figure is available in the online journal.)

However, the principle of fragmentation developed here should be equally applicable to cometary meteoroids.

For stony asteroidal meteoroids, K/μ can be determined from the samples collected on the ground. No such samples of cometary meteoroids can be obtained. Cometary meteoroids are believed to consist of a mixture of dust particles and frozen gases. One could perhaps estimate the value of K/μ from the values known for packed snow. For example, melting snow has a K value between 10^{-9} and 4×10^{-9} m^2 (Colbeck & Anderson, 1982). The viscosity of liquid nitrogen is about 10^{-4} N s m^{-2}. Assuming that this viscosity value for the fluid permeates through a cometary fragment, for a fragment 1 m in radius at an altitude of 40 km moving with a speed of 30 km s^{-1}, the incubation time τ_1 is about 0.1 s. This leads to a much larger survival rate of cometary meteoroids than predicted by Hills & Goda (1993). One might synthesize a comet-like material in a laboratory, and measure its K/μ. In any case, the present incubation time model should lead to more realistic values of the survival rates of cometary meteoroids.

Finally, it is interesting to examine the initial splitting velocity value deduced from the present ballistic range experiment, V_0, of 20 m s^{-1}. One can express the splitting velocity in the form

$$V_d = C \left(\frac{\rho}{\rho_s} \right)^{1/2} U.$$

Equation (4) assigned $C = 2$. The deduced value of 20 m s^{-1} corresponds to $C = 1.25$. Passey & Melosh (1980) deduced, from the sizes of the craters, $C = \sqrt{1.5} = 1.22$. Artem'eva & Shuvalov (2001) derived, through CFD calculations, $C = 0.5$. Thus, the present 20 m s^{-1} value is well within the expected range.

8. CONCLUSIONS

The experimental data obtained in a ballistic range show that fragmentation occurs at a much slower rate than predicted by the existing theory. A new hypothesis saying that the incubation process precedes the splitting process and that the incubation time is the time for the pressurized fluid to permeate through the fragment predicts a much slower fragmentation than predicted by the existing theory, at least for small fragments, and leads to a better agreement between the experiment and the calculation.

APPENDIX

NOMENCLATURE

K Permeability, m^2

n Local number density of fragments, m^{-3}

p Pressure, Pascal

r Radius of a fragment, m

r_0 Radius of fragments at start, m

R Fragment's distance from axis of symmetry, m

R_e Value of R at the outer edge of fragment cloud, m

t Time, s

u Velocity of permeating fluid, m s^{-1}

U Laboratory-relative axial velocity of a fragment, m s^{-1}

V Laboratory-relative normal velocity of a fragment, m s^{-1}

V_d Velocity gained by a fragment by splitting, m s^{-1}

V_0 The V-value at the outer edge of fragment cloud at start, m s^{-1}

x Axial distance within a fragment, m

W Magnitude of the relative velocity between air flow and fragment, m s^{-1}

Δt Time intervals along meteoroid trajectory, s

μ Viscosity, N s m^{-2}

ρ Local air density, kg m^{-3}

ρ_s Density of fragment, kg m^{-3}

τ Characteristic time for fragmentation, s

τ_1 Fragmentation incubation time, s

τ_2 Fragment splitting time, s

REFERENCES

Artem'eva, N. A., & Shuvalov, V. V. 1996, Shock Waves, 5, 359
Artem'eva, N. A., & Shuvalov, V. V. 2001, J. Geophys. Res., 106, 3297
Ashby, M. F., & Sammis, C. G. 1990, Pure Appl. Geophys., 3, 489

Baldwin, B., & Sheaffer, Y. 1971, J. Geophys. Res., 76, 4653
Borovicka, J., & Kalenda, P. 2003, Meteorit. Planet. Sci., 76, 4653
Colbeck, S. C., & Anderson, E. A. 1982, Water Resour. Res., 18, 904
Hills, J. G., & Goda, M. P. 1993, AJ, 105, 1114
Levin, B. Yu., & Bronshten, V. A. 1986, Meteoritics, 21, 199
Park, C. 2009, J. Thermophys. Heat Transfer, 23, 417
Park, C., & De Rose, C. E. 1980, Shape Change of Galileo Probe Models in Free-Flight Tests, NASA Technical Memorandum 81209
Passey, Q. R., & Melosh, H. J. 1980, Icarus, 42, 211
Shuvalov, V. V., & Trubetskaya, I. A. 2010, Sol. Syst. Res., 44, 104
Stone, J. M., & Norman, M. L. 1992, ApJS, 80, 753
Yamamoto, S. 2004, AIAA J., 42, 1849
Zhdan, I. A., Stulov, V. P., & Stulov, P. V. 2004, Dokl. Phys., 49, 315